Hindawi Publishing Corporation
Journal of Nanomaterials
Volume 2016, Article ID 3746861, 9 pages
http://dx.doi.org/10.1155/2016/3746861

Research Article

Double Walled Carbon Nanotube/TiO_2 Nanocomposites for Photocatalytic Dye Degradation

Alex T. Kuvarega and Bhekie B. Mamba

Nanotechnology and Water Sustainability Research Unit, College of Science, Engineering and Technology, University of South Africa, Florida Campus, Johannesburg, South Africa

Correspondence should be addressed to Alex T. Kuvarega; kuvarat@unisa.ac.za

Received 25 July 2016; Accepted 3 October 2016

Academic Editor: Rajesh Adhikari

Double walled carbon nanotube (DWCNT)/N,Pd codoped TiO_2 nanocomposites were prepared by a modified sol-gel method and characterised using FTIR, Raman spectroscopy, TGA, DRUV-Vis, XRD, SEM, and TEM analyses. TEM images showed unique pearl-bead-necklace structured morphologies at higher DWCNT ratios. The nanocomposite materials showed characteristic anatase TiO_2 Raman bands in addition to the carbon nanotube D and G bands. Red shifts in the UV-Vis absorption edge were observed at low DWCNT percentages. The photocatalytic activity of DWCNT/N,Pd TiO_2 nanocomposite was evaluated by the photocatalytic degradation of eosin yellow under simulated solar light irradiation and the 2% DWCNT/N,Pd TiO_2 nanocomposite showed the highest photoactivity while the 20% DWCNT/N,Pd TiO_2 hybrid was the least efficient. The photocatalytic enhancement was attributed to the synergistic effects of the supporting and electron channeling role of the DWCNTs as well as the electron trapping effects of the platinum group metal. These phenomena favour the separation of the photogenerated electron-hole pairs, reducing their recombination rate, which consequently lead to significantly enhanced photoactivity.

1. Introduction

The discovery of carbon nanotubes (CNTs) in the early 1990s revolutionalised research in a myriad of R&D fields such as nanoelectronics, biosensors, intercalation materials, supercapacitors, drug delivery, polymer composites, and catalysis [1]. The unique and outstanding mechanical and electronic properties of CNTs have provided new impetus in their potential application in semiconductor nanocomposites as photocatalysts for degradation of organic pollutant and bacteria as well as water splitting to generate hydrogen gas [2–4]. Their one-dimensional structure allows electrons to be conducted without being scattered, a phenomenon known as ballistic transport which permits the nanotube to conduct without dissipating energy as heat [5]. This property is quite enticing in the fabrication of CNT-semiconductor hybrids in which electron channeling through the CNT is desirable. The semiconductor characteristics of CNTs may also induce changes in the reactivity of supported semiconductor nanoparticles by electron transfer. Reports on Coulombic charge transfer between Pt and Au metal nanoparticles supported on the SWCNT and the semiconducting SWCNTs have been made [6]. The surface area of CNTs may range from over 1000 m^2/g for single walled carbon nanotubes (SWCNTs) to 700–800 m^2/g for double walled carbon nanotubes (DWCNTs) and 200–300 m^2/g for multiwall carbon nanotubes (MWCNTs). The large surface area provides spatial confinement of any attached nanoparticles and large supporting surface areas, leading to faster rates of redox reactions. SWCNTs and DWCNTs are thus preferable candidates for a number of applications; however, the lack of low cost mass production is still a limit to their practical use [7].

Titanium dioxide (TiO_2) has emerged as the most preferable among many photocatalysts because of its many desirable properties such as nontoxicity, strong oxidizing power, low cost, ready availability, and long term photostability [8]. However, application of TiO_2 is hindered by its large band gap (3.2 eV), which translates to use of high energy UV radiation for activation. Various innovations aimed at improving the photoefficiency of TiO_2 have been attempted,

including modifications with metals [9, 10] and nonmetals [11, 12]. Simultaneous introduction of nonmetals and metals as TiO_2 dopants (codoping) has also been attempted in an effort to improve visible light responsiveness and reduction in electron-hole recombination of the resulting codoped TiO_2 [13–15].

CNTs/TiO_2 nanocomposites have been reported to promote the separation of the electron-hole charges generated upon irradiation as well as shift the absorption edge of the nanocomposite to the visible region [16]. However, most studies have shown nonuniform coatings of TiO_2 on the CNTs, with some bare CNTs surfaces and random aggregates of TiO_2 on the CNT surface, thus compromising the efficiency of the nanocomposite [17]. Recent studies on CNT/TiO_2 nanocomposites are focused mainly on MWCNT/TiO_2 and SWCNT/TiO_2 hybrids [18–22]. In this work, a simple sol-gel technique is used to synthesize DWCNT/N,Pd codoped TiO_2 nanocomposites by anchoring N,Pd codoped TiO_2 on the surfaces of DWCNTs. The photocatalytic activity of the synthesized nanocomposite was evaluated by photocatalytic degradation of eosin yellow under simulated solar light irradiation.

2. Experimental

2.1. Synthesis, Purification, and Functionalisation of DWCNTs. A catalyst with the elemental composition $Mg_{0.94}Co_{0.05}Mo_{0.01}O$ was prepared through combustion of Mg and Co nitrates and hexaammonium heptamolybdate tetrahydrate in the presence of citric acid [23]. In a typical experiment, $Mg(NO_3)_2{\cdot}6H_2O$ (70.53 g), $Co(NO_3)_2{\cdot}6H_2O$ (4.29 g), $(NH_4)_6Mo_7O_{24}{\cdot}4H_2O$ (3.72 g), and citric acid (170.16 g) were dissolved in deionised water and the solution stirred at 150°C until the solution turned purplish. The solution was then placed in a crucible and heated in a furnace at 550°C overnight. The resulting fluffy khaki brown oxide was finely ground and used as a catalyst in the synthesis of DWCNTs. The catalyst (0.5 g) was loaded into a ceramic boat which was then placed in a quartz tube connected to the gases and heated in an electric furnace at 1000°C for 2 h. Hydrogen gas (H_2) and methane gas (CH_4) were passed through the catalyst at constant flow rates of 50 mL/min and 200 mL/min, respectively, for 2 h and then the furnace and methane gas were switched off and hydrogen flow was maintained until the furnace cooled down to about 400°C. The pristine DWCNTs containing carbonaceous impurities and unreacted metal catalyst particles were sonicated in concentrated HCl (150 mL) for 3 h and washed several times with deionised water, filtered, and then dried in an oven at 90°C. The purified DWCNTs (2 g) were functionalised by sonication in a mixture of concentrated H_2SO_4 and HNO_3 (1 : 3 by volume) at room temperature for 3 h. The oxidised DWCNTs were then washed several times with deionised water, filtered until the filtrate pH was 7, and then dried overnight at 90°C.

2.2. Preparation of DWCNT/N,Pd Codoped TiO_2 Nanocomposites. Functionalised DWCNTs were dispersed in a solution of 2-propanol C_3H_8O (50 mL) (99.8%, Sigma Aldrich, Germany) and titanium isopropoxide (TTIP) (10 mL) (97%, Sigma Aldrich, Germany). The mixture was sonicated for 30 minutes to improve CNT dispersion. Palladium diamine dichloride, $Pd(NH_3)_2Cl_2$, (45% Pd, PGM Chemicals, RSA) was then dissolved in 12 mL of aqueous ammonia (25%, Merck, Germany) to give a Pd : Ti ratio of 0.5% and added dropwise to the DWCNT/2-propanol/titanium isopropoxide mixture with vigorous stirring for 30 minutes and the precipitate was left to age for 4 hours. The suspension was then oven dried overnight at 80°C. The resulting powder was calcined in a furnace for 2 h at 450°C before characterisation. Nanocomposites containing 0.5%, 1%, 2%, 5%, 10%, and 20% DWCNTs were prepared by weighing appropriate amounts of oxidised DWCNTs and denoted NC-1 to NC-6, respectively.

2.3. Characterisation of the Materials. FTIR analysis was performed to probe the functional groups present on the materials. A Perkin Elmer Spectrum 100 was used. The nature of the DWCNTs and the nanocomposites was confirmed using a Raman microscope (Perkin Elmer RamanMicro 200). X-ray diffraction (XRD) analysis was performed at room temperature on a Philips PANanalytical X'pert operated at 40 kV and 40 mA. Optical properties were investigated in the reflectance mode on a Shimadzu UV-2540. Morphological properties were observed on a transmission electron microscope (TEM) (Tecnai G^2 Spirit) equipped with an INCA EDS analyser and scanning electron microscope (SEM) (NOVA FEI/FIB). Thermal properties were evaluated by thermogravimetric analysis (TGA) (Perkin Elmer TGA 4000) over a temperature range of 30°C–800°C.

2.4. Photocatalytic Activity Tests. A portion of the NC (0.1 g) was suspended in the dye (eosin yellow) solution (100 mL and 100 ppm) and stirred in the dark to allow for adsorption equilibrium for about an hour. An Oriel Newport 500 W Xenon lamp solar simulator equipped with an Air Mass 1.5 Global Spectral Filter was employed for sample irradiation. The power output was measured with an Oriel PV reference cell. Aliquots (2 mL) of the suspension were sampled at 15-minute intervals and filtered through a syringe filter and the dye concentration was determined using UV-Vis spectroscopy (Shimadzu UV-2450) at $\lambda = 515$ nm.

3. Results and Discussion

FTIR analysis confirmed the presence of OH groups centred at 3351 cm^{-1} due to carboxyl functionalisation of the DWCNTs. The band at 1461 cm^{-1} present in both pristine and oxidised DWCNTs was ascribed to the C=C stretching vibrations. The two bands at 1120 cm^{-1} and 1594 cm^{-1} correspond to C–O and C=O stretching of carboxyl groups, further confirming the DWCNTs were –COOH functionalised (Figure 1(a)). These become anchor sites for attachment of TiO_2 nanoparticles forming C–O–Ti linkages and thus the NC spectra were largely similar with the main peaks below 550 cm^{-1}, ascribed to the Ti–O–Ti and Ti–O–C vibrations (Figure 1(b)). Broad band peaks centred at around 3390 cm^{-1} confirmed the OH stretching of physisorbed water on the nanocomposite surfaces. Sharp bands at around 1630 cm^{-1}

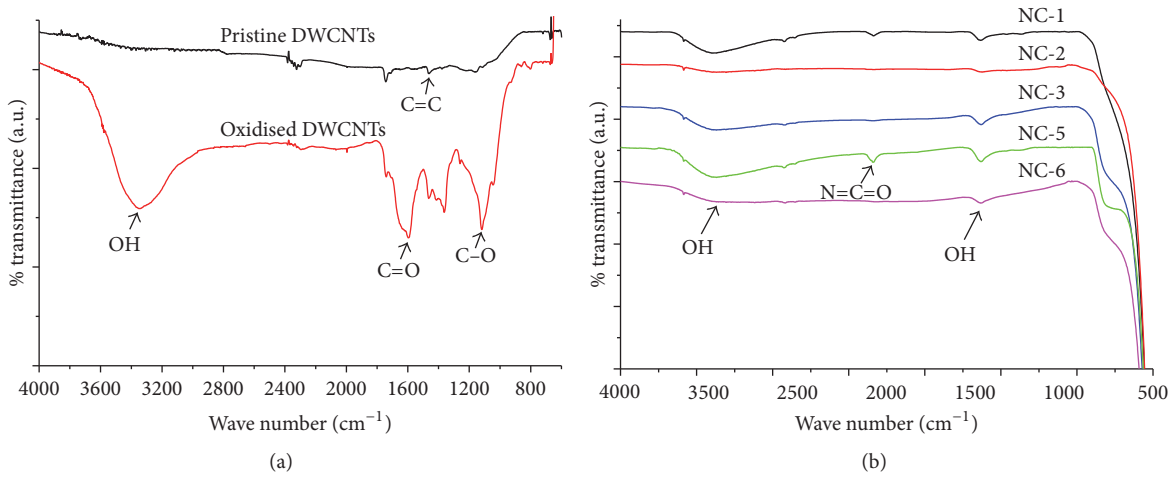

FIGURE 1: FTIR spectra of (a) pristine and oxidised DWCNTs and (b) nanocomposites.

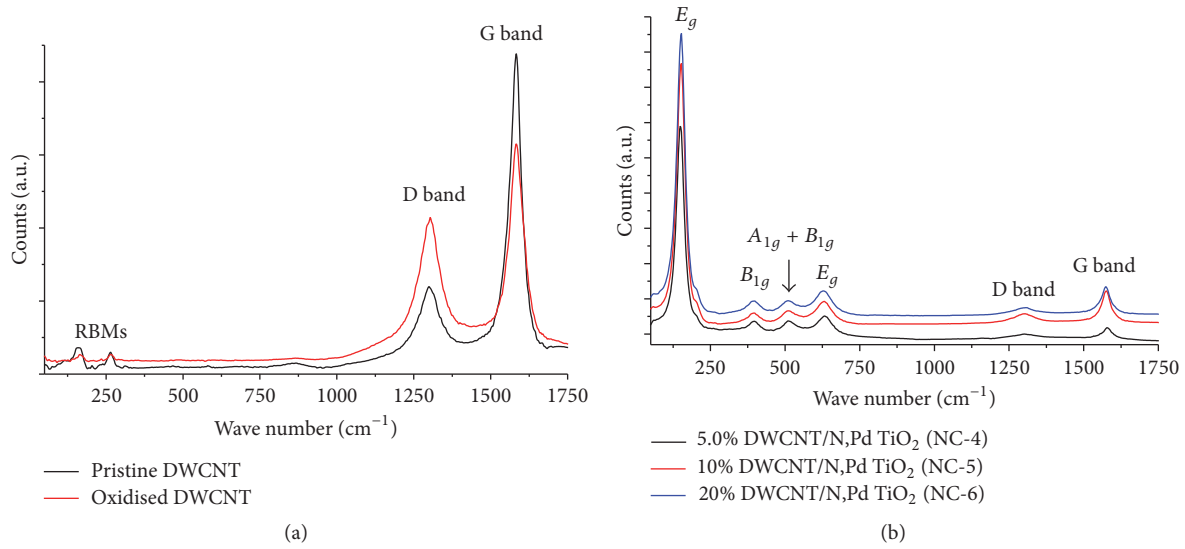

FIGURE 2: Raman spectra of (a) pristine and oxidised DWCNT showing the D and G bands as well as the RBMs and (b) nanocomposites.

were attributed to the OH bending modes of the water molecules. However, since ammonium hydroxide was used as the N precursor for the N,Pd codoped TiO_2, it also forms linkages with the available functional groups on the DWCNTs forming the N=C=O linkages with characteristic vibrations at 2350 cm^{-1}. Peaks associated with the functionalisation of DWCNTs were not observed in the nanocomposites. This could indicate formation of linkages between the DWCNTs and the TiO_2 which occurs through –COOH functionalities.

Raman spectra of pristine and oxidised DWCNTs showed radial breathing mode (RBM) vibrations in the low frequency region (100–400 cm^{-1}) in addition to the D (1305 cm^{-1}) and G bands (1582 cm^{-1}) (Figure 2(a)) [24]. The nanocomposites showed characteristic peaks for DWCNTs as well as anatase TiO_2 (Figure 2(b)). The D and G bands centred at 1299 cm^{-1} and 1572 cm^{-1}, respectively, were observed for NC-4 to NC-6. The slight decrease in the nanocomposite peak frequencies compared to the oxidised DWCNTs could indicate formation of Ti–O bonds with oxygen functional groups on the chemically oxidised DWCNTs. The lower frequency Raman region is dominated by the TiO_2 bands. Peaks centred at 151 cm^{-1}, 395 cm^{-1}, 510 cm^{-1}, and 636 cm^{-1} can be ascribed to the E_g, B_{1g}, unresolved $A_{1g} + B_{1g}$, and E_g Raman allowed modes of anatase TiO_2, respectively [25, 26].

X-ray diffraction patterns at 2θ values of 25.29, 37.83, 48.07, 54.14, 55.07, 62.64, 68.94, 70.14, and 75.11 can be indexed to the (101), (004), (200), (105), (211), (204), (116), (220), and (215) crystal planes of the anatase phase of TiO_2, respectively [27, 28] (Figure 3). The DWCNT peaks (expected at $2\theta = 25.6^{\circ}$) could not be detected due to possible overlap with the high intensity TiO_2 E_g peak [26].

Crystallite sizes (D) were estimated from the Scherrer equation:

$$D = \frac{k\lambda}{\beta \cos\theta}, \quad (1)$$

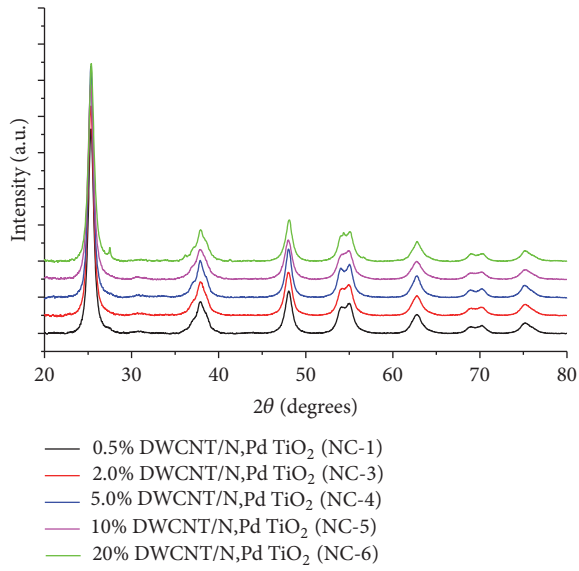

Figure 3: XRD patterns of the nanocomposites.

Table 1: Average crystallite sizes and band gaps.

Sample	Crystallite size (nm)	Direct band gap (eV)
NC-1	10.9	2.40
NC-2	10.6	2.70
NC-3	10.3	3.15
NC-4	11.8	2.65
NC-5	10.5	3.34
NC-6	11.6	3.36

where λ is the X-ray wavelength, β is the broadening of the peak, θ is the angle of diffraction, and k is a constant [15, 27]. The anatase (101) peak at $2\theta = 25.3^{\circ}$ was used to estimate the crystallite sizes. There were significant differences in crystallite sizes with increasing amounts of DWCNTs in the nanocomposites (Table 1). Similar studies on Fe/TiO_2-MWCNT composites reported average crystallite size of 5 nm [29].

Optical properties of the nanocomposites are shown in Figure 4(a). A fundamental absorption edge in the UV region, attributed to charge transfer from the valence to the conduction band of the TiO_2, is observed for all samples [30]. The strong UV absorption is accompanied by tailing well into the visible region which decreases in the midrange with increasing amount of DWCNTs in the nanocomposites. The strongest absorption in the visible region was observed for NC-1 centred at around 500 nm. Increasing the amount of DWCNTs in the nanocomposites resulted in a decrease in the absorption in the region around 500 nm but an increase was observed between 700 nm and 900 nm. Increase in visible light absorption can be explained by N doping which forms interband gap states in TiO_2, resulting in reduced band gap and consequently shifting the absorption edge to the visible region. The presence of Pd is also associated with absorption in the visible region due to d-d electron transitions [15]. CNTs are known to absorb well in the entire visible region, so their presence in the nanocomposites also contributes to enhanced visible light absorption. Controlling the composition ratio of DWCNTs in these nanocomposites is crucial for optimal synergistic effect between the DWCNTs and the codoped TiO_2. The band gap (E_g) of the materials was estimated from the Tauc plots by plotting $[F(R) \cdot h\nu]^n$ against $h\nu$ (Figure 4(b)). An increase in band gap energy with increasing percentages of DWCNTs in the nanocomposites (Table 1) was observed. Higher amounts of DWCNTs limit the available N and Pd for doping with TiO_2 as some of these elements may become associated with the DWCNTs, causing gradual increase in band gap. Lower band gaps (increased visible light absorption) were only achieved at lower DWCNT ratios.

SEM and TEM images of the oxidised and TiO_2 covered DWCNTs are shown in Figure 5. The DWCNTs appeared as long and narrow diameter tubes (Figures 5(a) and 5(b)). SEM images of the NC-5 show clusters of codoped TiO_2 surrounding the DWCNTs to form rough tubular structures (Figure 5(c)) The diameter of the nanocomposites was visibly larger than that of the oxidised DWCNTs due to TiO_2 coverage. The length of the nanocomposites was shorter than that of the oxidised DWCNTs suggesting possible shortening during the sol-gel processing. The formation of TiO_2 aggregates confirmed the role of the DWCNTs as support for the deposition and growth or spatial confinement of the N,Pd codoped TiO_2 clusters. TEM image of the nanocomposite (NC-5) shows TiO_2 particles anchored onto the small diameter DWCNTs to form long pearl-bead-necklace-like structures (Figure 5(d)). The bead-like TiO_2 particle coverage indicates strong contact with the DWCNTs. The average size of the anchored TiO_2 nanoparticles is about 10 nm.

EDS analysis was performed on one of the nanocomposites (NC-3) to probe the elemental composition of the material (Figure 6). The presence of Ti, O, Pd, and C confirmed the existence of Pd doped TiO_2 on the DWCNTs. The intensity of the C peak was much lower compared to the Ti and O peak intensities, suggesting near complete coverage of the DWCNTs by the TiO_2 concurring with SEM and TEM observations. Pd showed the lowest peak intensity as expected because of the low levels (0.5%) used in preparing the materials. The Si could have originated as a contaminant from the glassware while the Cu signal came from the copper grid used as the sample support during TEM analysis.

Thermograms of the nanocomposites show a small weight loss (about 2%) below 100°C, attributed to the adsorbed water molecules on the materials (Figure 7). A weight loss at around 550°C can be attributed to the loss of the graphitic skeleton of DWCNTs in the nanocomposites. The total carbon loss at this temperature reveals the percentage DWCNTs in the respective nanocomposites and the residual percentage weight gives an approximate amount of N,Pd TiO_2 in the nanocomposites. The percentage weight loss values at 550°C are lower than those predicted from the starting precursor materials. This may be due to the bundling together and aggregation of the DWCNTs, a prominent phenomenon at higher CNT percentages.

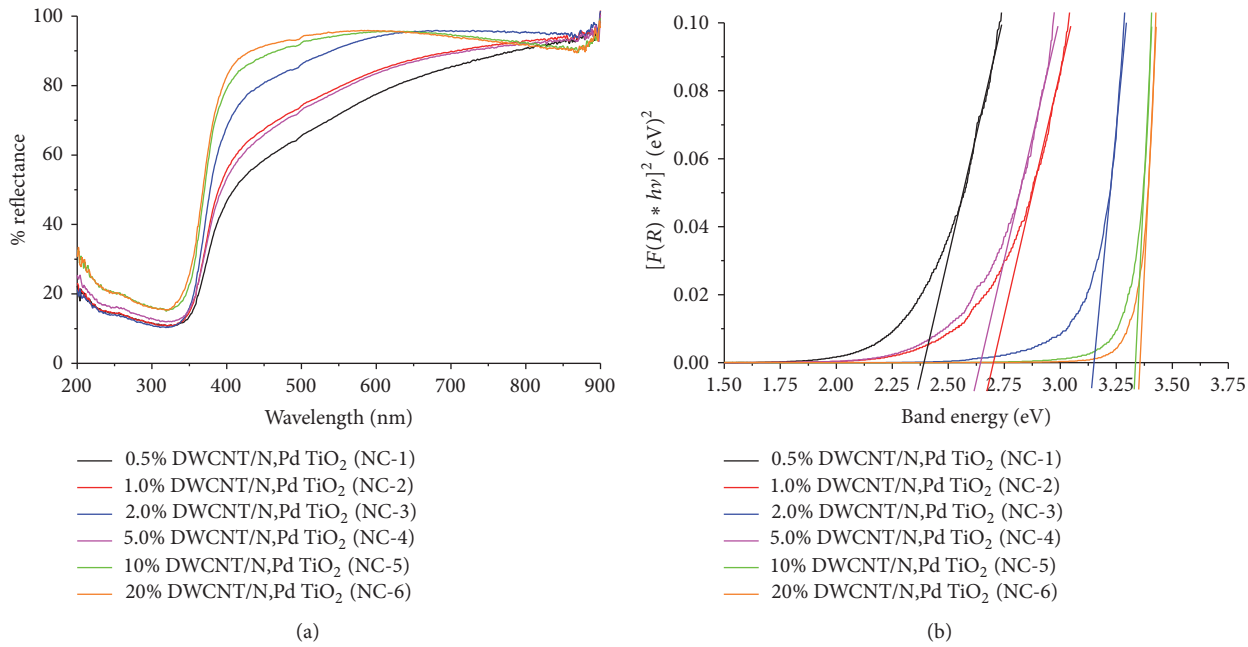

(a) (b)

Figure 4: (a) Reflectance spectra and (b) Tauc plots of the nanocomposites.

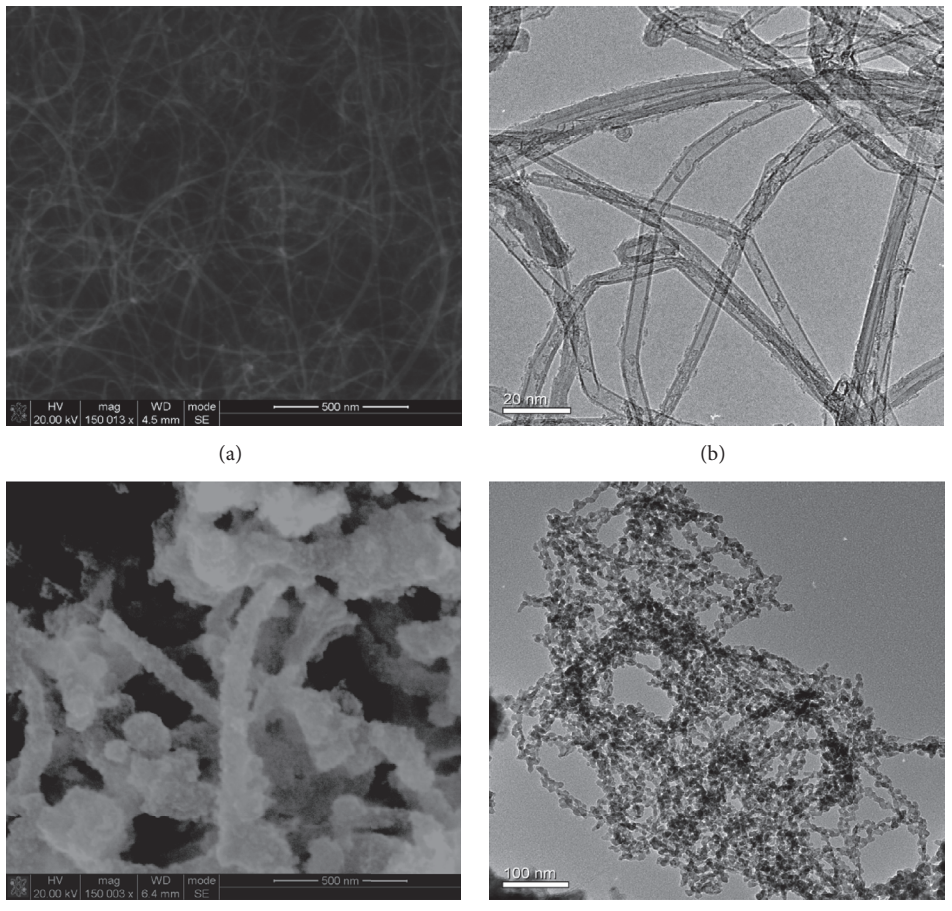

(a) (b)

(c) (d)

Figure 5: SEM images of (a) functionalised DWCNT, (c) NC-5, and TEM images of (b) functionalised DWCNT, (d) NC-5.

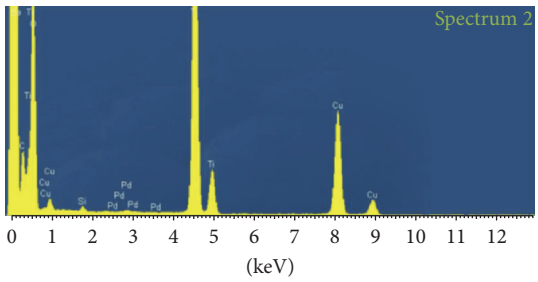

Figure 6: EDS spectrum of NC-3.

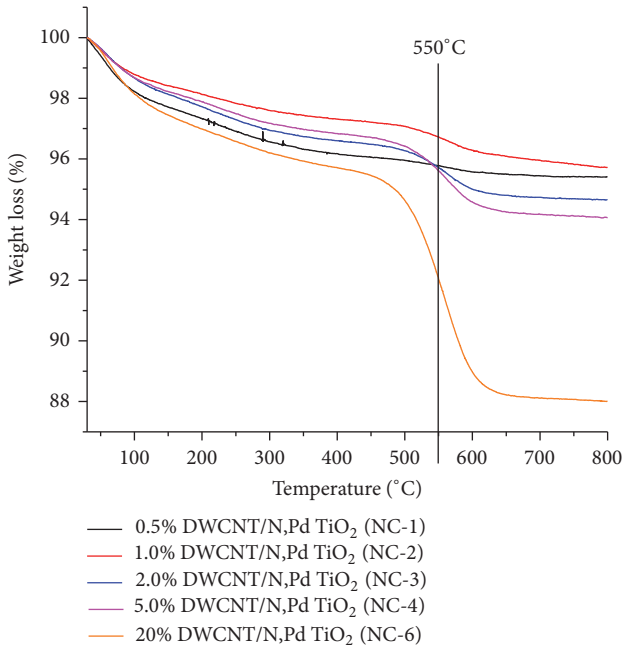

Figure 7: Thermograms of the nanocomposites.

Dye degradation was evaluated from the measured concentrations of the sampled dye aliquots at 15-minute intervals using the following equation:

$$\text{Dye degradation} = \frac{C_t}{C_0}, \quad (2)$$

where C_t and C_0 are the concentrations of dye at reaction time t and 0, respectively.

Reaction kinetics data were computed from the simplified Langmuir-Hinshelwood kinetics model, assuming first order kinetics:

$$-\ln\left(\frac{C}{C_0}\right) = kt, \quad (3)$$

where k is the apparent rate constant and t is time.

Photocatalytic evaluation of the nanocomposites showed the highest activity for the NC-3 (Figure 8(a)). Initially there was an increase in degradation efficiency with increasing amount of DWCNT and then a decrease at much higher DWCNT percentages. Photocatalytic enhancement can be explained in terms of DWCNT/N,Pd TiO_2 heterojunctions that help reduce the rate of the recombination of photogenerated charge carriers. There is also possibility of shifting of the TiO_2 apparent Fermi level thereby allowing the utilisation of low energy photons for photo activation. Presence of DWCNTs promotes excellent charge transfer ability, high surface area for increased dye adsorption, and the formation of Ti–C bonds between the CNTs and TiO_2, resulting in enhanced visible light absorption [30–32].

DWCNTs themselves can also absorb photons, get excited, and inject electrons into the TiO_2 conduction band, triggering the formation of highly reactive superoxide and hydroxyl radicals [33]. The decrease in photoactivity at higher DWCNT percentages correlated well with the increase in band gaps estimated from the Tauc plots. From the observed trend, it can be postulated that there is an optimum DWCNT/TiO_2 ratio that offers the best conditions for the synergy between DWCNTs and N,Pd TiO_2 in the nanocomposites. The photodegradation kinetics followed pseudo first order kinetics postulated from the Langmuir-Hinshelwood model (Figure 8(b)). Dye adsorption, degradation, and apparent rate constants are summarised in Table 2. In a study on CNT/TiO_2 nanocomposites with different CNT loadings, the optimum CNT/TiO_2 ratio was found to be in the range from 1.5% to 5% by weight [33]. A study on the degradation of acetone using TiO_2/CNT nanocomposites gave an optimal amount of TiO_2 and CNTs in the range of 10 : 1 and 5 : 1 [34].

Table 2: Dye adsorption, degradation, and apparent rate constants.

Sample	Dye adsorption (%)	Degradation after 180 min (%)	Rate constant, k_{app} (min^{-1})
NC-1	6.03	98.25	1.904×10^{-2}
NC-2	8.10	99.00	2.148×10^{-2}
NC-3	9.93	99.87	3.220×10^{-2}
NC-4	6.38	99.17	2.263×10^{-2}
NC-5	11.18	98.27	1.697×10^{-2}
NC-6	8.56	96.34	1.370×10^{-2}

A rate constant of 3.220×10^{-2} min^{-1} observed for NC-3 (2.0% DWCNT/N,Pd TiO_2) is higher compared to the one reported for similar work performed using MWCNT/N,Pd TiO_2 nanocomposites [15, 35]. However, both results reveal an improvement compared to commercial TiO_2 (P25) which was used as a reference under similar conditions (Table 3). N doped and N,Pd codoped TiO_2 performed better than the P25 with N,Pd codoped TiO_2 showing even better performance than when incorporated into CNTs. The NC-3 showed a rather mixed order reaction kinetics shown by the S shaped curve. This can be attributed to the presence of both pearl-bead-necklace structures as well as formation of aggregates on the DWCNTs surface.

UV-Vis scans of the dye photodegradation ware plotted as a function of irradiation time for the NC-6 (Figure 9) and no new absorption peaks were observed. This confirmed that the dye was completely mineralised.

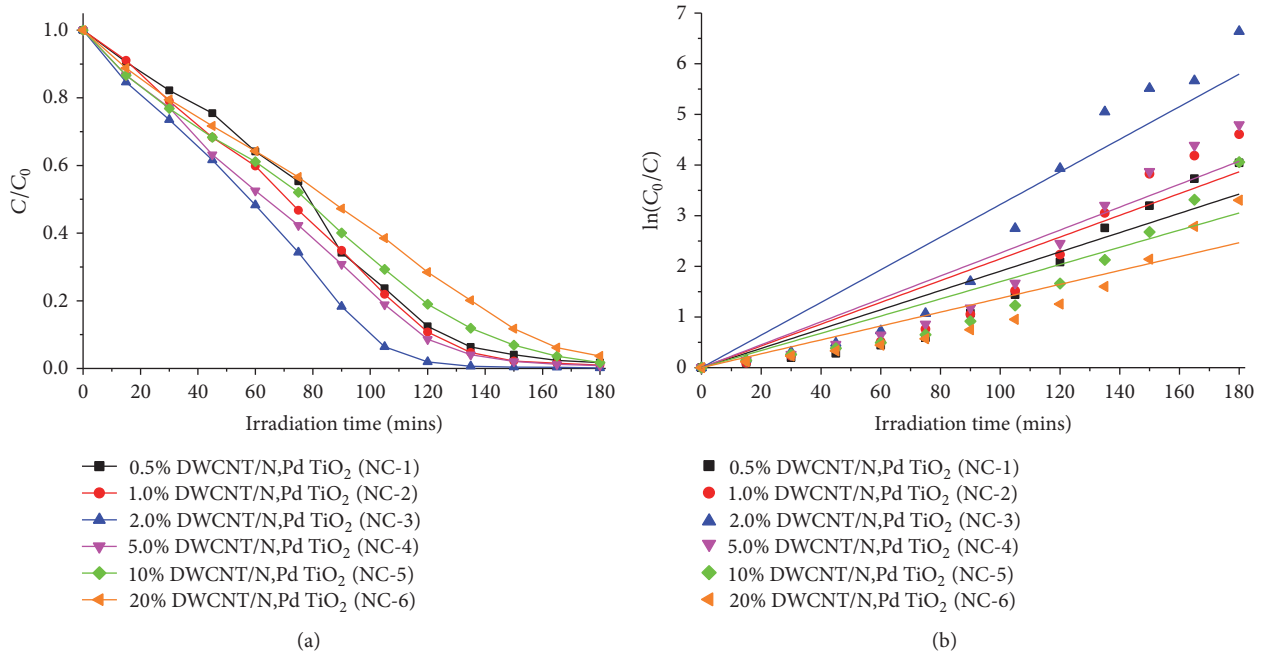

Figure 8: (a) Photodegradation profiles and (b) photodegradation kinetics of EY under simulated solar irradiation.

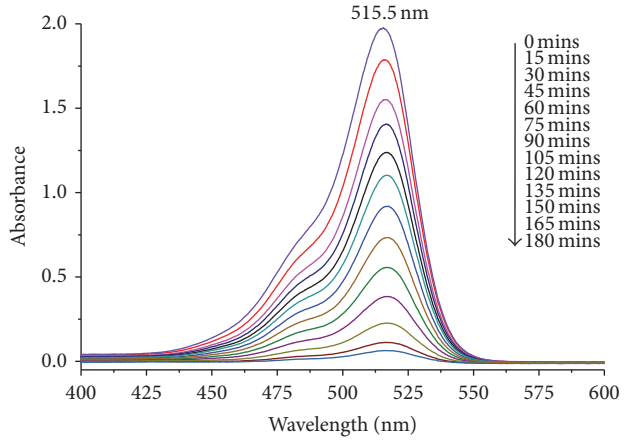

Figure 9: Eosin yellow photodegradation profiles of NC-6.

Table 3: Rate constants of other photocatalysts.

Material	Apparent rate constant, k_{app} (min^{-1})
Comm. TiO_2 (P25)	3.96×10^{-3}
N doped TiO_2	1.41×10^{-2}
N,Pd TiO_2	3.84×10^{-2}
2.0% MWCNT/N,Pd TiO_2 (0.5% Pd)	1.34×10^{-2}
2.0% DWCNT/N,Pd TiO_2 (0.5% Pd)[a]	2.22×10^{-2}

[a]Results of this study.

A mechanism for the photocatalytic enhancement was proposed based on substitution of O by N in the TiO_2 lattice resulting in formation of interband gap states and therefore facilitating the use of less energetic visible light to activate the TiO_2 (Figure 10). Pd becomes an electron sink due to the formation of a Schottky barrier at the semiconductor metal interface [2, 36]. DWCNTs act as effective electron transfer channels due to their high electrical conductivity. They exhibit high electron capture ability and high electron storage capacity and can act as super capacitors [37]. DWCNTs can also act as photosensitisers, because of their semiconductive properties, absorbing visible light radiation and transferring the photogenerated electrons into the conduction band of the N,Pd codoped TiO_2 particles [38]. The resulting positively charged DWCNTs can capture electrons from the valence band of N,Pd codoped TiO_2, thereby extending the lifetime of holes.

4. Conclusion

Anchoring N,Pd codoped TiO_2 on DWCNTs led to changes in the morphology and optical properties of the composite materials resulting in enhanced photocatalytic activity of the nanocomposites towards degradation of eosin yellow. The ability of DWCNTs and Pd to act as electron sinks highlights their mediating roles in the charge transfer process. DWCNTs also reduce N,Pd codoped TiO_2 agglomeration and induce synergistic effects on the photocatalytic performance. Photocatalytic enhancement was only observed at low DWCNT : Ti ratio of 2.0% by weight. DWCNT/N,Pd codoped TiO_2 are promising candidates for addressing some of the fundamental issues in many practical environmental applications including removal of organic pollutants from water.

Competing Interests

The authors declare no conflict of interests regarding the publication of this article.

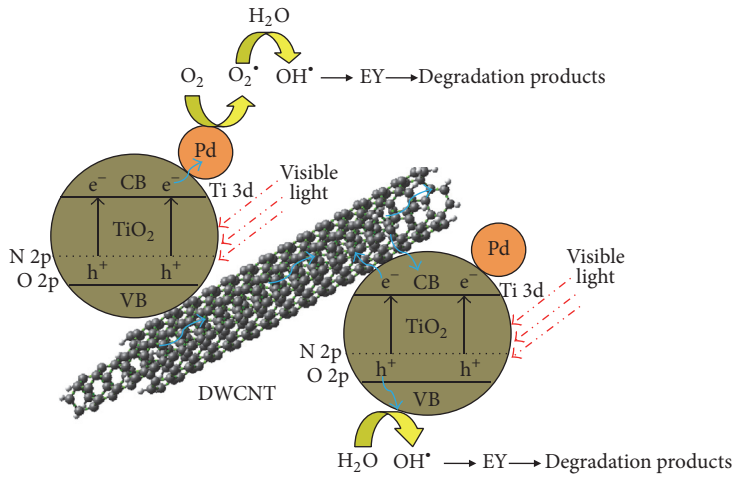

Figure 10: Proposed photocatalytic mechanism of the nanocomposites.

Acknowledgments

The authors acknowledge funding from the Nanotechnology and Water Sustainability Research Unit (NanoWS), University of South Africa (UNISA).

References

[1] Y. Zhang, Z.-R. Tang, X. Fu, and Y.-J. Xu, "Engineering the unique 2D mat of graphene to achieve graphene-TiO_2 nanocomposite for photocatalytic selective transformation: what advantage does graphene have over its forebear carbon nanotube?" *ACS Nano*, vol. 5, no. 9, pp. 7426–7435, 2011.

[2] K. Woan, G. Pyrgiotakis, and W. Sigmund, "Photocatalytic carbon-nanotube-TiO_2 composites," *Advanced Materials*, vol. 21, no. 21, pp. 2233–2239, 2009.

[3] J. H. Park, S. Kim, and A. J. Bard, "Novel carbon-doped TiO_2 nanotube arrays with high aspect ratios for efficient solar water splitting," *Nano Letters*, vol. 6, no. 1, pp. 24–28, 2006.

[4] V. B. Koli, A. G. Dhodamani, A. V. Raut, N. D. Thorat, S. H. Pawar, and S. D. Delekar, "Visible light photo-induced antibacterial activity of TiO_2-MWCNTs nanocomposites with varying the contents of MWCNTs," *Journal of Photochemistry and Photobiology A: Chemistry*, vol. 328, no. 1, pp. 50–58, 2016.

[5] H. J. Li, W. G. Lu, J. J. Li, X. D. Bai, and C. Z. Gu, "Multichannel ballistic transport in multiwall carbon nanotubes," *Physical Review Letters*, vol. 95, no. 8, Article ID 086601, 2005.

[6] R. Voggu, S. Pal, S. K. Pati, and C. N. R. Rao, "Semiconductor to metal transition in SWNTs caused by interaction with gold and platinum nanoparticles," *Journal of Physics: Condensed Matter*, vol. 20, no. 21, Article ID 215211, 2008.

[7] D. S. Su, S. Perathoner, and G. Centi, "Nanocarbons for the development of advanced catalysts," *Chemical Reviews*, vol. 113, no. 8, pp. 5782–5816, 2013.

[8] K. Rajasekar, S. Thennarasu, R. Rajesh, R. Abirami, K. Balkis Ameen, and A. Ramasubbu, "Preparation of mesoporous TiO_2/CNT nanocomposites by synthesis of mesoporous titania via EISA and their photocatalytic degradation under visible light irradiation," *Solid State Sciences*, vol. 26, pp. 45–52, 2013.

[9] H. Chen, M. Shen, R. Chen, K. Dai, and T. Peng, "Photocatalytic degradation of commercial methyl parathion in aqueous suspension containing La–doped TiO_2 nanoparticles," *Environmental Technology*, vol. 32, no. 13, pp. 1515–1522, 2011.

[10] J. Zhou, Y. Zhang, X. S. Zhao, and A. K. Ray, "Photodegradation of benzoic acid over metal-doped TiO_2," *Industrial and Engineering Chemistry Research*, vol. 45, no. 10, pp. 3503–3511, 2006.

[11] Y. Cong, J. Zhang, F. Chen, and M. Anpo, "Synthesis and characterization of nitrogen-doped TiO_2 nanophotocatalyst with high visible light activity," *The Journal of Physical Chemistry C*, vol. 111, no. 19, pp. 6976–6982, 2007.

[12] J. Wang, D. N. Tafen, J. P. Lewis et al., "Origin of photocatalytic activity of Nitrogen-doped TiO_2 nanobelts," *Journal of the American Chemical Society*, vol. 131, no. 34, pp. 12290–12297, 2009.

[13] Y. Sakatani, J. Nunoshige, H. Ando et al., "Photocatalytic decomposition of acetaldehyde under visible light irradiation over La^{3+} and N Co-doped TiO_2," *Chemistry Letters*, vol. 32, no. 12, pp. 1156–1157, 2003.

[14] Y. Cong, J. Zhang, F. Chen, M. Anpo, and D. He, "Preparation, photocatalytic activity, and mechanism of nano-TiO_2 Co-doped with nitrogen and iron (III)," *The Journal of Physical Chemistry C*, vol. 111, no. 28, pp. 10618–10623, 2007.

[15] A. T. Kuvarega, R. W. M. Krause, and B. B. Mamba, "Nitrogen/palladium-codoped TiO_2 for efficient visible light photocatalytic dye degradation," *The Journal of Physical Chemistry C*, vol. 115, no. 45, pp. 22110–22120, 2011.

[16] Z. Li, B. Gao, G. Z. Chen, R. Mokaya, S. Sotiropoulos, and G. Li Puma, "Carbon nanotube/titanium dioxide (CNT/TiO_2) core–shell nanocomposites with tailored shell thickness, CNT content and photocatalytic/photoelectrocatalytic properties," *Applied Catalysis B: Environmental*, vol. 110, pp. 50–57, 2011.

[17] R. Leary and A. Westwood, "Carbonaceous nanomaterials for the enhancement of TiO_2 photocatalysis," *Carbon*, vol. 49, no. 3, pp. 741–772, 2011.

[18] H. Langhuan, W. Houjin, L. Yingliang, J. Zibin, and S. Zibei, "TiO_2/carbon nanotube composites and their synergistic effects on enhancing the photocatalysis efficiency," *Progress in Chemistry*, vol. 22, no. 5, pp. 867–876, 2010.

[19] M. Wongaree, S. Chiarakorn, and S. Chuangchote, "Photocatalytic improvement under visible light in TiO_2 nanoparticles by carbon nanotube incorporation," *Journal of Nanomaterials*, vol. 2015, Article ID 689306, 10 pages, 2015.

[20] S. Da Dalt, A. K. Alves, and C. P. Bergmann, "Photocatalytic degradation of methyl orange dye in water solutions in the presence of MWCNT/TiO_2 composites," *Materials Research Bulletin*, vol. 48, no. 5, pp. 1845–1850, 2013.

[21] S. Da Dalt, A. K. Alves, F. A. Berutti, and C. P. Bergmann, "Designing of TiO_2/MWCNT nanocomposites for photocatalytic degradation of organic dye," *Particulate Science and Technology*, vol. 33, no. 3, pp. 308–313, 2015.

[22] Y. Yao, G. Li, S. Ciston, R. M. Lueptow, and K. A. Gray, "Photoreactive TiO_2/carbon nanotube composites: synthesis and reactivity," *Environmental Science & Technology*, vol. 42, no. 13, pp. 4952–4957, 2008.

[23] E. Flahaut, A. Peigney, W. S. Bacsa, R. R. Bacsa, and C. Laurent, "CCVD synthesis of carbon nanotubes from (Mg,Co,Mo)O catalysts: influence of the proportions of cobalt and molybdenum," *Journal of Materials Chemistry*, vol. 14, no. 4, pp. 646–653, 2004.

[24] E. Flahaut, C. Laurent, and A. Peigney, "Catalytic CVD synthesis of double and triple-walled carbon nanotubes by the control of the catalyst preparation," *Carbon*, vol. 43, no. 2, pp. 375–383, 2005.

[25] L. De Luca, A. Donato, S. Santangelo et al., "Hydrogen sensing characteristics of Pt/TiO_2/MWCNTs composites," *International Journal of Hydrogen Energy*, vol. 37, no. 2, pp. 1842–1851, 2012.

[26] Z. Peining, A. S. Nair, Y. Shengyuan, and S. Ramakrishna, "TiO_2-MWCNT rice grain-shaped nanocomposites—synthesis, characterization and photocatalysis," *Materials Research Bulletin*, vol. 46, no. 4, pp. 588–595, 2011.

[27] P. Panagiotopoulou and D. I. Kondarides, "Effect of morphological characteristics of TiO_2-supported noble metal catalysts on their activity for the water-gas shift reaction," *Journal of Catalysis*, vol. 225, no. 2, pp. 327–336, 2004.

[28] G. Jiang, X. Zheng, Y. Wang, T. Li, and X. Sun, "Photo-degradation of methylene blue by multi-walled carbon nanotubes/TiO_2 composites," *Powder Technology*, vol. 207, no. 1–3, pp. 465–469, 2011.

[29] K. Zhang and W.-C. Oh, "Kinetic study of the visible light-induced sonophotocatalytic degradation of MB solution in the presence of Fe/TiO_2-MWCNT catalyst," *Bulletin of the Korean Chemical Society*, vol. 31, no. 6, pp. 1589–1595, 2010.

[30] L. Tian, L. Ye, K. Deng, and L. Zan, "TiO_2/carbon nanotube hybrid nanostructures: solvothermal synthesis and their visible light photocatalytic activity," *Journal of Solid State Chemistry*, vol. 184, no. 6, pp. 1465–1471, 2011.

[31] K. Dai, X. Zhang, K. Fan, T. Peng, and B. Wei, "Hydrothermal synthesis of single-walled carbon nanotube-TiO_2 hybrid and its photocatalytic activity," *Applied Surface Science*, vol. 270, pp. 238–244, 2013.

[32] M.-L. Chen, J.-S. Bae, H.-S. Yoon, C.-S. Lim, and W.-C. Oh, "The photodegradation effect of organic dye for metal oxide (Cr_2O_3, MgO and V_2O_3) treated CNT/TiO_2 composites," *Bulletin of the Korean Chemical Society*, vol. 32, no. 3, pp. 815–820, 2011.

[33] B. Gao, G. Z. Chen, and G. Li Puma, "Carbon nanotubes/titanium dioxide (CNTs/TiO_2) nanocomposites prepared by conventional and novel surfactant wrapping sol-gel methods exhibiting enhanced photocatalytic activity," *Applied Catalysis B: Environmental*, vol. 89, no. 3-4, pp. 503–509, 2009.

[34] W. Wang, P. Serp, P. Kalck, and J. L. Faria, "Visible light photodegradation of phenol on MWNT-TiO_2 composite catalysts prepared by a modified sol-gel method," *Journal of Molecular Catalysis A: Chemical*, vol. 235, no. 1-2, pp. 194–199, 2005.

[35] A. T. Kuvarega, R. W. M. Krause, and B. B. Mamba, "Multiwalled carbon nanotubes decorated with nitrogen, palladium co-doped TiO_2 (MWCNT/N, Pd co-doped TiO_2) for visible light photocatalytic degradation of Eosin Yellow in water," *Journal of Nanoparticle Research*, vol. 14, no. 4, article 776, 16 pages, 2012.

[36] Z. Zhang and J. T. Yates Jr., "Band bending in semiconductors: chemical and physical consequences at surfaces and interfaces," *Chemical Reviews*, vol. 112, no. 10, pp. 5520–5551, 2012.

[37] A. Kongkanand and P. V. Kamat, "Electron storage in single wall carbon nanotubes. Fermi level equilibration in semiconductor-SWCNT suspensions," *ACS Nano*, vol. 1, no. 1, pp. 13–21, 2007.

[38] M.-L. Chen, F.-J. Zhang, and W.-C. Oh, "Synthesis, characterization, and photocatalytic analysis of CNT/TiO_2 composites derived from MWCNTs and titanium sources," *New Carbon Materials*, vol. 24, no. 2, pp. 159–166, 2009.